Research Article | Vol. 32, No. 6 / 11 Mar 2024 / Optics Express 9589

Optics EXPRESS

All-optical Stern-Gerlach effect in the time domain

GIL BASHAN, AVISHAY EYAL, MOSHE TUR, AND ADY ARIE*

School of Electrical Engineering, Fleischman Faculty of Engineering, Tel Aviv University, Tel Aviv 69978, Israel
*ady@tauex.tau.ac.il

Abstract: The Stern-Gerlach experiment, a seminal quantum physics experiment, demonstrated the intriguing phenomenon of particle spin quantization, leading to applications in matter-wave interferometry and weak-value measurements. Over the years, several optical experiments have exhibited similar behavior to the Stern-Gerlach experiment, revealing splitting in both spatial and angular domains. Here we show, theoretically and experimentally, that the Stern-Gerlach effect can be extended into the time and frequency domains. By harnessing Kerr nonlinearity in optical fibers, we couple signal and idler pulses using two pump pulses, resulting in the emergence of two distinct eigenstates whereby the signal and idler are either in phase or out of phase. This nonlinear coupling emulates a synthetic magnetization, and by varying it linearly in time, one eigenstate deflects towards a higher frequency, while the other deflects towards a lower frequency. This effect can be utilized to realize an all-optical, phase-sensitive frequency beam splitter, establishing a new paradigm for classical and quantum data processing of frequency-bin superposition states.

1. Introduction

The Stern-Gerlach (SG) experiment [1–9] is a pillar in quantum physics, providing compelling evidence for the quantum behavior of the spin angular momentum of the electron. In that experiment, a beam of silver atoms passing through a non-uniform transverse magnetic field was split into two distinct directions, representing the two eigenstates of this system, where the spin is either parallel or anti-parallel to the direction of the magnetic field gradient. Several SG-type experiments have been proposed and conducted using light waves [10–19], exhibiting splitting effects like the original SG experiment. Recently, several studies have developed theoretical frameworks [20,21] and demonstrated [22,23] SG-type experiments in the field of nonlinear optics, specifically in the context of $\chi^{(2)}$ three waves mixing. These studies have revealed the splitting of an input signal (or idler) beam into two distinct directions, representing the two eigenstates of the system. These works relied on second order nonlinearity in non-centro-symmetric crystals and resulted in splitting in the space/spatial-frequency domain. Here instead, we report a SG-type splitting in the time/temporal-frequency domain, based on a third order nonlinear effect (four-wave mixing) in optical fibers.

The underlying dynamics of all the above-mentioned systems is that of coupled two-level system. In the case of sum frequency generation in nonlinear crystals, the (undepleted) pump couples between the signal and idler [24–28], whereas in the case of four-wave mixing (FWM) in optical fibers, two undepleted pumps couple between them [29–32]. This enabled to observe effects such as adiabatic frequency conversion, and accumulation of adiabatic geometric phase, first in quadratic nonlinear systems [24,25,33,34] and more recently using FWM [29,30,32,35]. An important difference, however, is that the interacting beams in bulk nonlinear crystals undergo diffraction, whereas in fibers we consider interacting pulses that undergo dispersion.

Here we utilize the analogy between diffraction and dispersion phenomena [36–38] to analyze and demonstrate a temporal SG-type experiment, enabling the all-optical control of the splitting

#510722 https://doi.org/10.1364/OE.510722
Journal © 2024 Received 31 Oct 2023; revised 15 Jan 2024; accepted 9 Feb 2024; published 4 Mar 2024

Optics EXPRESS

of signals in the time-frequency domain, using commercially available telecom components (see Fig. 1). The observation of this SG-like effect has significant potential for data manipulation in both the classical and quantum optical regimes. In the classical regime, the ability to shift a pair of pulses spectrally or temporarily can be beneficial for optical signal processing applications. In the quantum regime, it opens the door for creation and splitting of frequency bin entangled states [30–32,39–45], based on their relative phase. These states are highly important for quantum information processing since they represent the outputs of a Hadamard gate when the input is either a photon at the signal frequency or the idler frequency.

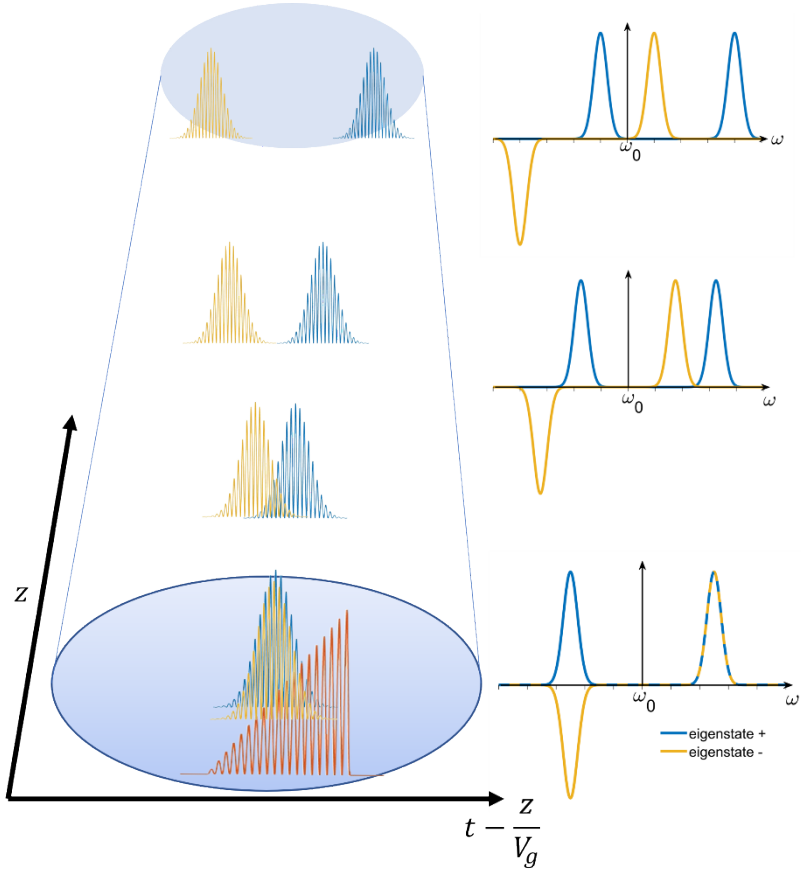

Fig. 1. The principle of the all-optical Stern-Gerlach effect in the time domain. Two pump tones within a common ramp pulsed envelope (red line) couple light between signal and idler pulses. This interaction gives rise to two distinct eigenstates (blue and orange lines), where the signal and idler exhibit the same phase in one eigenstate and opposite phases in the other eigenstate (see bottom right illustration). As these pulses propagate in the fiber, the eigenstates experience frequency domain splitting (right side) and subsequently, temporal splitting into opposite directions (left side) owing to their propagation in the dispersive fiber.

2. Results

2.1. Theoretical analysis

Two strong optical pump pulses propagating in a nonlinear material can couple between relatively weak signal and idler pulses [29–32,42], under the energy conservation condition

Optics EXPRESS

$\omega_{p1} - \omega_{p2} = \omega_i - \omega_s$ where $\omega_{p1}, \omega_{p2}, \omega_i, \omega_s$ represent the angular frequencies of the two pumps, idler and signal, respectively. Neglecting common phase changes between the signal and idler via cross phase modulation (XPM) and, assuming undepleted pumps (see Supplementary section), the evolution of the signal and idler wavepackets can be described by the coupled wave equations (CWE) [46,47].

$$\frac{\partial^2}{\partial\tau^2}A_i - \frac{2i}{\beta_2}\frac{\partial A_i}{\partial z} = \frac{4}{\beta_2}\gamma A_s A_{p1} A_{p2}^* \exp(i\Delta k z) \tag{1}$$

$$\frac{\partial^2}{\partial\tau^2}A_s - \frac{2i}{\beta_2}\frac{\partial A_s}{\partial z} = \frac{4}{\beta_2}\gamma A_i A_{p2} A_{p1}^* \exp(-i\Delta k z) \tag{2}$$

Here A_{p1}, A_{p2}, A_i, A_s represent the slowly varying complex envelopes of the two pumps, idler, and signal waves, respectively. The variable $\tau = t - z/V_g$ denotes the retarded time frame, i.e. the time delay it takes for the signal and idler to travel a distance of z at a group velocity of V_g, where z is the propagation coordinate. The above two equations therefore describe the evolution of the signal and idler wavepackets in a frame that moves at the group velocity. Assuming that the spectral separation between the signal and idler waves is sufficiently small, the group velocity dispersion (GVD) parameters, β_2, and V_g remain identical for both waves. The Kerr nonlinear coefficient, γ, is expressed in units of $W^{-1}m^{-1}$, and $\Delta k = k_{p1} - k_{p2} + k_s - k_i$ denotes the wavenumber mismatch term, where k_{p1}, k_{p2}, k_s, k_i are the wavenumbers of the two pumps, signal, and idler, respectively. By introducing normalized fields in the rotating frame, $\psi_{i/s} = (|A_i|^2 + |A_s|^2)^{-\frac{1}{2}} \exp(\mp i\Delta k z/2) A_{i/s}$, the CWEs can be written in matrix form, with position independent coupling matrix:

$$i\frac{\partial}{\partial z}\begin{pmatrix}\psi_i\\ \psi_s\end{pmatrix} = \left(\frac{\beta_2}{2}\mathbf{p}_\tau^2 - \vec{\sigma}\cdot\vec{M}\right)\begin{pmatrix}\psi_i\\ \psi_s\end{pmatrix} \tag{3}$$

In Eq. (3), $\mathbf{p}_\tau = -\frac{\partial}{\partial\tau}$ represents the temporal equivalent of the momentum operator, $\vec{\sigma} = (\sigma_x, \sigma_y, \sigma_z)$ represents the Pauli matrix vector, and the temporal synthetic magnetism [27], $\vec{M} = 2|\gamma A_{p1} A_{p2}^*|(\hat{x}\cos(\phi) + \hat{y}\sin(\phi)) + \hat{z}\Delta k/2$ is defined by the phase difference$\phi = \phi_{\mathrm{p2}} - \phi_{\mathrm{p1}}$ between the two pumps. Equation (3) is mathematically equivalent to the transverse Pauli equation, which describes a nonrelativistic spin ½ particle subjected to a weak transverse magnetic field (as used in the original Stern-Gerlach experiment[1]). The key distinction between the transverse Pauli equation and Eq. (3) lies in the exchange between time and position (see Supplementary section for details). Consequently, in the case of time dependent synthetic magnetism, we can anticipate temporal and frequency splitting rather than direction and spatial splitting.

In order to realize the all-optical SG effect in the time domain, a phase matching condition must be satisfied, and the synthetic magnetism $\vec{M}$ should exhibit a uniform temporal slope that overlaps with the signal and idler pulses. This can be achieved by modulating the pump pulses in a manner similar to a ramp pulse, which has a duration longer than that of the signal and idler pulses. This modulation allows the synthetic magnetism absolute value to be approximated by a first-order Taylor series, represented as $|\vec{M}| = M_0 + M'\tau$. In Fourier space Eq. (3) can be diagonalized, resulting in two eigenstates:

$$|\psi_+\rangle = \frac{|\psi_s\rangle + e^{-i\phi}|\psi_i\rangle}{\sqrt{2}} \quad , \quad |\psi_-\rangle = \frac{|\psi_s\rangle - e^{-i\phi}|\psi_i\rangle}{\sqrt{2}} \tag{4}$$

Here, spinor and bra-ket notations have been employed. Note that the signal-only $|\psi_s\rangle$ (or idler only $|\psi_i\rangle$) wavepackets are not eigenstates of this system. Generally, the incident spinor $|\psi_{incident}\rangle$ in the frequency domain can be expressed as a superposition of the eigenstates: $|\psi_{incident}\rangle = (\cos(\theta)\exp(\mathrm{i}\delta)|\psi_+\rangle + \sin(\theta)|\psi_-\rangle) \otimes \int \mathrm{d}\omega\ a_i(\omega)|\omega\rangle$. Where δ is an arbitrary phase,

Optics EXPRESS

$a_i(\omega)$ represents the Fourier space envelope for the signal and idler components, typically modeled as Gaussian pulses with $a_i(\omega) = \mathrm{A}_0\left(\sqrt{\pi}\ \ \Delta\omega\right)^{-1} \exp(-\omega^2/2\Delta\omega^2)$, where $\Delta\omega$ denotes the pulse bandwidth. The spinor as function of propagation coordinate z can be expressed in terms of the effective propagator, $\exp(-izH_\pm)$, as $|\psi\rangle(z,\omega) = (\exp(-izH_+)|\psi_+\rangle\langle\psi_+| + \exp(-izH_-)|\psi_-\rangle\langle\psi_-|)|\psi_{incident}\rangle$, where $H_\pm = -\frac{\beta_2}{2}\omega^2 \mp \frac{1}{2}M_0 \mp iM'\frac{\partial}{\partial\omega}$ denote the two effective Hamiltonians corresponding to the two eigenstates of Eq. (5). The propagator itself can be calculated using Zassenhaus formula [21,48]:

$$\exp(-izH_\pm) = \exp\left(\mp iz\frac{1}{2}M_0 + \frac{1}{6}i\beta_2 z^3 M'^2\right)\exp\left(\pm zM'\frac{\partial}{\partial\omega}\right)\exp\left(iz\frac{\beta_2}{2}\omega^2 \mp \frac{1}{2}i\beta_2 z^2 M'\omega\right) \tag{5}$$

Here the term $\exp\left(\pm zM'\frac{\partial}{\partial\omega}\right)$ is the translation operator in the Fourier space. Therefore, the optical angular frequency of the first eigenstate $|\psi_+\rangle$ increases by zM', while decreasing by the same amount for the second eigenstate $|\psi_-\rangle$. Consequently, when the incident spinor $|\psi_{incident}\rangle$ is not a pure eigenstate but rather a superposition of the two eigenstates, the spectrum will split into two shifted spectra (up-shifted and down-shifted). The intensity of each spectrum will depend on the relative weight of the corresponding eigenstate in the incident spinor. The term $\exp(\mp i\beta_2 z^2 M'\omega/2)$ introduces a time shift with direction that varies with the eigenstates. Hence, in the case of an incident spinor that is a superposition of the eigenstates (e.g., a signal only, or idler only spinor), the pulses will exhibit temporal splitting. The term $\exp(\mp izM_0/2)$ represents a different phase accumulation for each eigenstate that may create Rabi oscillations between the signal and the idler, that are characteristic phenomenon of two-level systems. These oscillations result from interference between the two eigenstates, hence, when the incident spinor is a pure eigenstate there is no oscillation.

Figure 2 displays a simulation illustrating the impact of the translation operator in the frequency domain and the Rabi oscillation of the signal and idler over a length of 8 times the characteristic nonlinear length [46], $L_{NL} = 1/\gamma P_p$ where P_p represents the geometric mean of the power of the pumps that overlaps with the signal and idler. The slope was 2.5 $W\cdot ns^{-1}$. The simulation assumes $|A_{p1}| = |A_{p2}|$ and ignores second order effects, in order to clarify the role of the components in the propagator. Panels (a) and (b) show the power spectral density (PSD) of the signal or idler when the spinor state is $|\psi_+\rangle$ and $|\psi_-\rangle$, respectively. The dashed white line, featured in all panels, indicates the frequency shift in the presence of XPM only, $\Delta f_{XPM} = M'L/\pi$, excluding the temporal SG effect. The insets in all the figures present the PSD, as function of frequency, at $z = 1.85L_{NL}$ (marked by a dashed pink line). Comparing panels (a) and (b) demonstrates how each eigenstate undergoes a frequency shift of the same magnitude but in the opposite direction, while the envelope of the PSD remains unchanged. The frequency shifts are determined by the XPM and temporal SG effects $\Delta f = \Delta f_{SPM} \pm M'L/2\pi$. Panels (c) and (d) present the normalized PSD of the idler and signal, respectively, where the incident spinor is an equal superposition of the two eigenstates (the phase between signal and idler φ, equal 90 degrees), resulting in observable splitting in the frequency domain. Notably, in addition to the frequency splitting, the simulation also demonstrates the presence of Rabi oscillations between the signal and the idler in the initial stages. However, as the length L exceeds $4L_{NL}$, the frequency splitting becomes substantial, resulting in a lack of spectral overlap between the two eigenstates and, consequently, the decay of the Rabi oscillations. It should be noted that the frequency domain splitting presented in Fig. 2 and throughout the article is analogous to the splitting observed in the transverse spatial frequency (k) space in the original SG experiment. In the original SG experiment, the silver atom beams were measured at a distance from the magnetic field, effectively capturing the splitting in the k space, caused by the magnetic field gradient.

Optics EXPRESS

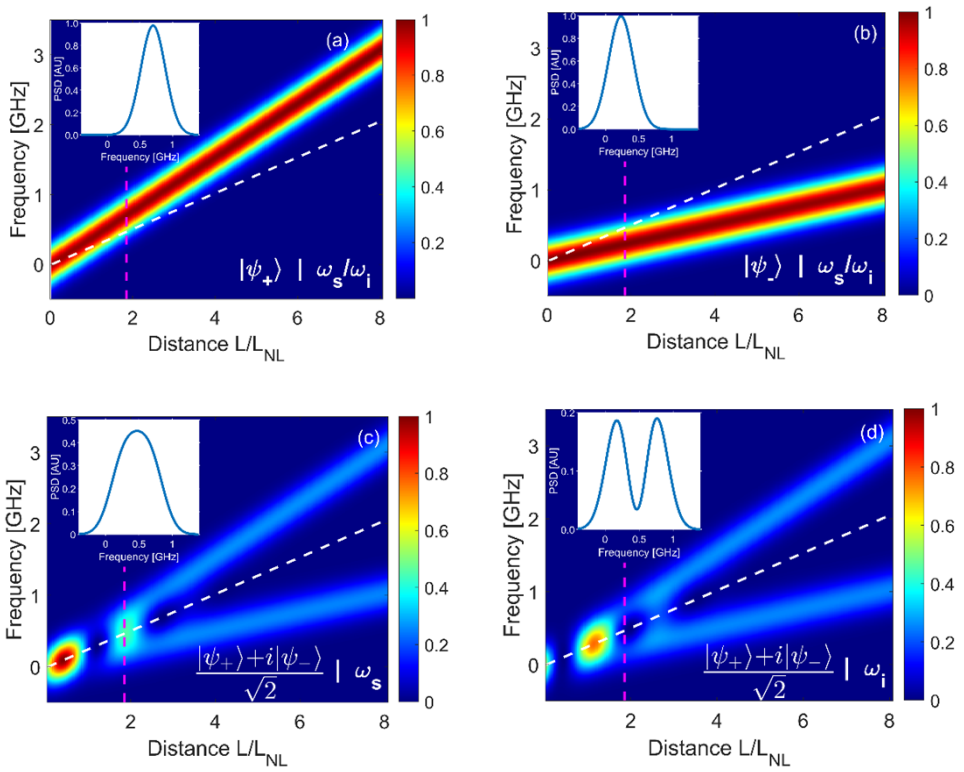

Fig. 2. Simulated signal and idler PSD along distance. a, the signal (or idler) in the eigenstate $|\psi_+\rangle$ exhibits a linear frequency-shift with length, the shift is higher than the XPM frequency shift, illustrated by the dashed white line. The envelope of the PSD remains constant during propagation. The inset shows the calculated PSD at $L = 1.85L_{NL}$ (marked with a dashed pink line). b, similar to panel (a) but for the eigenstate $|\psi_-\rangle$, demonstrating a linear frequency shift that is lower than the XPM frequency shift. (c) and (d), signal and idler PSD, respectively, in the eigenstates' superposition $(|\psi_+\rangle + i|\psi_-\rangle)/2$. The spectra exhibit splitting corresponding to the two eigenstates (showcased in panels (a) and (b)). Prior to the splitting, when the two eigenstates overlap in frequency, Rabi oscillation between the signal and idler is observed.

2.2. *Experimental results*

The experimental demonstration of the all-optical Stern-Gerlach effect in the time domain was conducted, and the corresponding setup and procedures are described in the Methods section. The employed pumps' wavelength was approximately 1552 nm, with a frequency spacing of 10 GHz between the two pumps. The total duration of the pump pulses was 3.8 ns. Their envelopes were tailored such that they included a linear power ramp in a 2 ns time interval that overlapped with the signal and the idler. (see Fig. 6(b) in the Methods section). The signal and idler wavelengths were around 1550 nm, while their frequency difference matched that of the two pump pulses. The signal and idler pulses were generated as Gaussian waveforms, characterized by a full width at half maximum (FWHM) of 1 ns. The phase difference (φ) between the signal and idler waves could be controlled, thus generating a spinor that is either one of the two eigenstates or any superposition of them.

The nonlinear medium employed in the experiment was a standard single-mode telecom fiber with a length of 1 km. The investigation of the optical frequency shifts for both the signal and the idler relied on the technique of self-heterodyne detection [49]. However, the temporal shift

Optics EXPRESS

was too minute to be detected under the prevailing experimental conditions. This scenario resembles the original Stern-Gerlach experiment, where the screen was placed at a significant distance from the magnetic field, facilitating the detection of changes in momentum direction rather than alterations in spatial configuration within the magnetic field. Figure 3 presents the experimental and simulated PSD of the signal (left side) and idler (right side) as a function of frequency deviation from the carrier. Note that neither of these two states is an eigenstate of the system. The pump peak power was 700 mW with slope of approximately 0.35 $W \cdot ns^{-1}$. The data have been normalized, with the maximum PSD set to 1. The solid blue line represents the experimental results, while the dashed red line corresponds to the simulation. There is a close agreement between the experimental and simulated outcomes. The traces in panel (a) reveal that the spectrum of the pure state $|\psi_+\rangle$ (Assuming, without loss of generality, a pump phase difference of $\phi = 0$, yields φ=0) undergoes a shift towards higher frequencies by 0.27 GHz compared to the pure state $|\psi_-\rangle$ ($\varphi = 180$ degrees) observed in panel (c). For all superpositions of the eigenstates, the spectrum exhibits dependence on the relative weighting of each eigenstate, which in turn is influenced by the phase (panels (b), (d)). In panel (b) ($\varphi = 80$ *degrees*), it is observed that the idler component experiences destructive interference between the two spectra

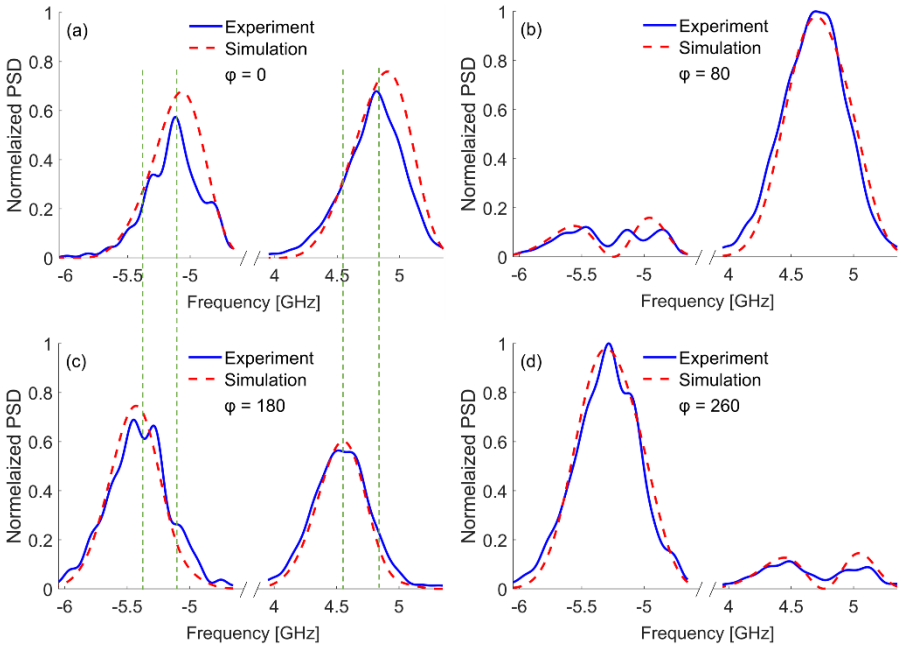

Fig. 3. Experimental and simulation results of the PSD of the signal and idler at various phase differences. The horizontal axis represents the frequency distance from the optical carrier. Each panel shows the signal on the left and the idler on the right. The blue line represents the experimental data, while the dashed red line corresponds to the simulation results. a, phase different between the signal and the idler $\varphi = 0$ degrees corresponding to the eigenstate $|\psi_+\rangle$. b, phase difference $\varphi = 80$ degrees, which is not an eigenstate of the system, resulting in a varying PSD envelope. The idler exhibits constructive interference between the two eigenstates, while the signal demonstrates destructive interference via Rabi oscillation. c, Phase difference $\varphi = 180$ degrees, corresponding to the eigenstate $|\psi_+\rangle$. The dashed green lines illustrate the frequency distance between the two eigenstates in panels (a) and (c) caused by SG splitting. d, Phase difference $\varphi = 260$ degrees, similar to panel (b), this is not an eigenstate of the system. However, in this case the signal shows constructive interference, while the idler experiences destructive interference.

Optics EXPRESS

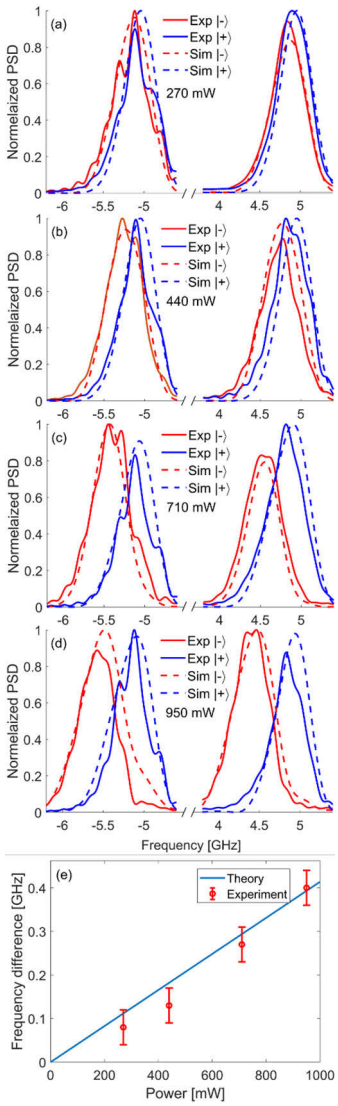

Fig. 4. Experimental and simulation results of the spectral deflection of the eigenstates' PSD. In panels a-d the horizontal axis is the same as Fig. 3, in the left side is the signal and in the right side is the idler. The blue lines represent the eigenstate $|\psi_+\rangle$, while the red lines exhibit the eigenstate $|\psi_-\rangle$. The solid lines are experiments and the dashed lines are simulation. a, the peak power was 270 mW and the frequency offset between the eigenstates is 0.08 GHz. b, the peak power was 440 mW and the frequency offset between the eigenstates is 0.13 GHz. c, the peak power was 710 mW and the frequency offset between the eigenstates is 0.27 GHz. d, the peak power was 950 mW and the frequency offset between the eigenstates is 0.4 GHz. e, the frequency splitting is plotted against the pump peak power. The solid blue line represents the theoretical model, while the red markers correspond to the data obtained from the panels shown above.

Optics EXPRESS

corresponding to the two eigenstates, whereas the signal component demonstrates constructive interference. Conversely, in panel (d) ($\varphi = 260$ *degrees*), the opposite behavior is observed. This phenomenon arises due to the Rabi oscillation occurring between the signal and idler components. In addition to the splitting observed between the two eigenstates, there is a frequency shift that is common to both eigenstates. This shift is attributed to the common XPM induced by the pumps on both the signal and idler components. Note that the phenomena depicted in this figure are consistent with those observed in the insets of Fig. 2.

Figure 4 shows the experimental and simulated PSD of the two eigenstates, as a function of pump power, with the blue lines corresponding to $|\psi_+\rangle$ and the red line to $|\psi_-\rangle$. The left side of the figure represents the signal component, while the right side corresponds to the idler component. The solid line represents the experimental results, while the dashed line corresponds to the simulation.

In panel (a), where the pump power is low (270 mW), the observed splitting is minimal. As the pump power increases, as in panels (b) and (c) the spectrum progressively splits into two distinct spectral peaks. Panel (d) demonstrates a splitting measurement of 0.4 GHz at a peak pump power of 950 mW. Panel (e) shows the theoretical frequency splitting as a function of pump power (indicated by a blue line), while the experimentally observed splitting is presented in panels (a-d) using red markers. The theoretical and experimental observations demonstrate close agreement. This observed splitting is a clear manifestation of an all-optical Stern-Gerlach effect in the time domain.

3. Discussion

In the above measurements, we showed that the frequency splitting between the two eigenstates increases with pump power. However, there is a practical limit to it. As the pump power increases, (unwanted) high order tones of the signal and idler appear. This limits the pump power level and consequently the frequency shift. One potential solution to overcome this challenge is to replace the standard telecom fiber with a dispersion-engineered fiber or dispersion shifted fiber and adjusting the wavelength to achieve phase matching with the signal and idler, while avoiding phase matching with high order tones [30,32,42]. Another approach is to explore the use of multimode fibers or polarization maintaining fibers. The phase accumulation can be adjusted using the intensity-dependent refractive index [47], which has the potential to enable phase matching only for the signal and idler components while the high order tones are not phase-matched. By employing these strategies, the adverse impact of high order tones can be mitigated, thereby enhancing the overall effectiveness of the system. Operating at pump powers levels, beyond the undepleted pump approximation [28], is another future direction to achieve high efficiency.

The pulses of the pump signal and idler that we utilized in this study had a duration on the nanosecond scale. These durations are already comparable to those used in state-of-the-art Quantum Key Distribution (QKD) [50]. Moreover, it is possible to further reduce the pulse durations by one order of magnitude, to match those of typical of high-speed optical communications. In that case, the spectral linewidth of the signal and idler would increase, but the corresponding pump's slope would also increase, consequently, the deflection of the signal and idler would increase. Thus, the crucial point to note is that the frequency deflection (or splitting) relative to the spectral linewidth of the pulses would remain unchanged.

The utilization of phase-sensitive frequency shifting, as analyzed and demonstrated in our study, introduces new capabilities for manipulating frequency-encoded optical information. It acts as a frequency-bin splitter, which exhibits sensitivity to phase and can be controlled by pump pulses. These features open interesting potential applications in the fields of classical optics and quantum optics. Specifically, it may enable frequency domain Hong–Ou–Mandel bunching of distinguishable signal and idler photons [20,40–43]. By sending an input state

Optics EXPRESS

$(|1_i 1_s\rangle)$ into the temporal SG system, these photons will bunch to one of the two eigenstates, $(|2_+0_-\rangle + |0_+2_-\rangle)/\sqrt{2}$, where $|2_\pm\rangle$ denote two photons (idler and signal photons) in the eigenstates $|\pm\rangle$.

The Hadamard gate, transforming two orthogonal input states $|0\rangle, |1\rangle$ to new orthogonal output states in a mutually unbiased base $(|0\rangle + |1\rangle)/\sqrt{2}$, $(|0\rangle - |1\rangle)/\sqrt{2}$, plays a crucial role in enabling quantum algorithms to simultaneously explore multiple possibilities and extract valuable information efficiently [51,52]. However, directly detecting the state of a single basis in the Hadamard basis in the frequency-bin is challenging. To address this, the Stern-Gerlach effect in the time domain, which is sensitive to phase and can distinguish between the two orthogonal base vectors of the Hadamard basis, may be employed. Figure 5 provides a schematic illustration of this effect. Since frequency-bin quantum information processing and communication are well-suited for transmission in SMF, the ability to apply the temporal Stern-Gerlach effect in SMF is significant.

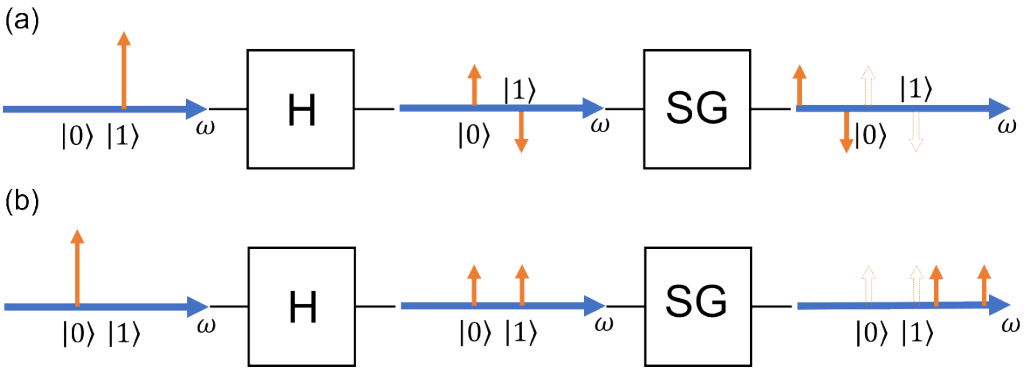

Fig. 5. Illustration of temporal SG effect for the Hadamard basis in the frequency-bin. a, (a) When a photon is initially in the $|1\rangle$ state at the input of the Hadamard gate, it undergoes a transformation to the $(|0\rangle - |1\rangle)/\sqrt{2}$ state. The temporal SG effect causes a deflection of the photon towards lower frequencies. b, Conversely, when a photon is initially in the $|0\rangle$ state at the input of the Hadamard gate, it undergoes a transformation to the $(|0\rangle + |1\rangle)/\sqrt{2}$ state. The temporal SG effect causes a deflection of the photon towards higher frequencies.

4. Summary

In this paper, we present the first analysis and demonstration of SG splitting in the time-frequency domain. Our study establishes an analogy between the Pauli equation and the signal-idler coupling via two pump pulses (Eq. (3)) in a Kerr nonlinear media. We show that a time-dependent nonlinear coupling gradient, that may be induced by the time gradient of the pump pulses, results in an optical frequency shift. The direction of the shift depends on the phase difference between the signal and the idler, while the magnitude of the shift is determined by the strength of the nonlinear coupling gradient and the length of the nonlinear material. Notably, this is the first analysis of an SG-type experiment in the context of third order nonlinearity. Since $\chi^{(3)}$ exists in centrosymmetric materials, including silicon and silica, this phenomenon can be observed in standard silica optical fibers, allowing for exploitation of long lengths of nonlinear interaction. Moreover, it may also enable to observe it in integrated-optics platforms, e.g., in silicon-photonics devices. Potential applications of the temporal SG effect are in classical and quantum optical communication systems. In particular, this effect enables to split orthogonal frequency bin qubits in the Hadamard basis.

Optics EXPRESS

5. Methods

5.1. Setup

The experimental setup used in demonstration of the all-optical Stern-Gerlach effect in the time domain is illustrated in Fig. 6 (a). A tunable laser diode at 1552 nm wavelength and 100 kHz linewidth served as the source of pumps light. The light was modulated into repeating ramp-shaped pulses of approximately 2 ns (see Fig. 6 (b)) duration and 35 ns period using an electro-optic amplitude modulator. The pumps pulses were subsequently amplified by a pre-amp erbium-doped fiber amplifier (EDFA). The pump pulses were then modulated again with electro-optic amplitude modulator, driven by a sine wave at frequency of Ω = 5 GHz. The modulator is biased for carrier suppression. Consequently, the modulator output comprised two ramp pulses separated by a frequency difference of 10 GHz (see Fig. 6 (c)).

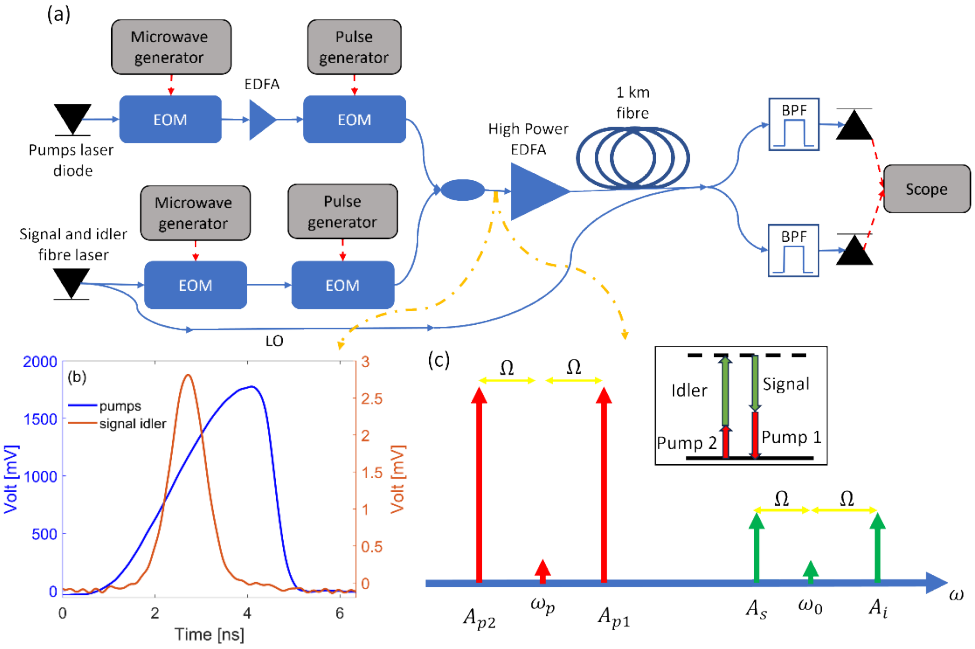

Fig. 6. Schematic illustration of the experimental setup. a, Pump light from a diode laser is initially modulated by an Electro-optic amplitude modulator (EOM) to generate a ramp pulse. The pulse is then amplified by an erbium-doped fiber amplifier (EDFA) and further modulated with a sine wave of Ω=2π·5 GHz using a second EOM biased for carrier suppression. The signal and idler light from a fiber laser are modulated by another EOM to generate Gaussian pulses and then modulated by a fourth EOM under the same conditions as the second EOM, with the tunable phase of the sine wave. The pump, signal, and idler are combined and amplified using EDFA. After combining the four tones, the light is coupled to a 1 km fiber. The combined light is then combined with a local oscillator (LO) replica of the signal and idler fiber lasers. Optical bandpass filters (BPF) are utilised to filter out the pumps and the signal/idler, and the LO and idler/signal are detected by fast photoreceivers and digitised using an oscilloscope. b, shows the measurement of the envelopes of the signal, idler, and pump pulses. c, provides a schematic illustration of their frequency domains and energy conservation.

A fiber laser operating at a wavelength of 1550 nm and with a linewidth of 1 *kHz* was split into two paths. The light in one arm served as the source for the signal and idler. Using another electro-optic amplitude modulator, the light was modulated into repeating Gaussian pulses with

Optics EXPRESS

FWHM of 1 ns, matching the period of the pump pulses (see Fig. 6 (b)). Similar to the pump pulses, the signal and idler pulses were subsequently modulated using an electro-optic amplitude modulator, biased for carrier suppression and driven by a sine wave at a fixed frequency of $\Omega = 5\ GHz$ and with adjustable phase. Consequently, the modulator output consisted of two gaussian pulses separated by a frequency difference of 10 GHz and a controllable phase difference, where the higher frequency pulse was designated as the idler and the other pulse as the signal.

The signal and idler pulses were combined with the pump pulses, aligning them on the slope of the pump pulses (see Fig. 6 (b)) while ensuring all fields shared the same polarization. Subsequently, the combined pulses underwent amplification to variable power levels, ranging in the order of hundreds of milliwatts, utilizing an EDFA. The amplified pulses were then coupled into a one-kilometer single-mode fiber. Simultaneously, light from the same fiber laser in the other path served as the local oscillator (LO) and was combined with the signal and idler pulses at the far end of the one-kilometer fiber. The wavenumber mismatch term Δk can be approximated as $\Delta k \approx 2\beta_2 \Delta\omega\Omega$, where $\Delta\omega$ denote the frequency difference between the pumps laser carrier and the signal and idler laser carrier. The corresponding nonlinear coherence length[45] is $L_{ch} = \pi/\Delta k \approx 1.6\ km$ which exceeds the length of the fiber used in the experiment. The differential group delay of the fiber was on the order of 0.1 $ps \cdot km^{-1/2}$, resulting in the nearly parallel polarization of the signal, idler, and pumps along the 1 km fiber. The broadening of the pulses owing to fiber dispersion is negligible in this experiment, since for the $\tau = 1\ ns$ pulses of the signal and idler, the dispersion length is $\tau^2/|\beta_2| = 50,000 km$ thus greatly exceeding the 1 km length of fiber that was used.

At the output port, the pump pulses were filtered using a fiber-coupled bandpass filter with a bandwidth of 0.8 nm. After that, the signal, idler, and LO were split into two optical fiber-coupled band-pass filters (BPF) with a bandwidth of less the 10 GHz, that allowed only the LO and the signal/idler to pass through. The LO is a continuous-wave signal, hence the beating signal appears on the oscilloscope only when the signal arrives. The filtered signals were then detected using photoreceivers with a rise time of 35 ps and responsivity of 4.4 VW^{-1}, and sampled by a digitizing oscilloscope at a sampling rate of 16 Giga-samples per second. Consequently, the detected voltage exhibited a central frequency of 5 GHz, in addition to the frequency offset caused by the all-optical Stern-Gerlach effect in the time domain. The Fourier transform of the detecting signal was calculated offline in order to calculate the PSD of the signal and idler. Due to the difficulty in accurately detecting the pump power in the experiment, we employed simulations to determine the power values.

5.2. Numerical calculations

The simulation in this study employs the split-step Fourier method as the underlying computational approach [46,53,54]. Initially, the idler and signal fields are non-chirped Gaussian pulses, while the pumps are modeled as 2 ns duration ramp pulses. The simulation in the experimental result section considers the potential formation of higher order tones of the signal and idler during propagation. Furthermore, it incorporates the consideration of small phase mismatch that occurs in the fiber due to chromatic dispersion. The simulation utilizes the following parameter values: a GVD parameter of $\beta_2 = -20\ ps^2\ km^{-1}$, a Kerr nonlinear coefficient of $\gamma = 1.3\ W^{-1}\ km^{-1}$, and a loss coefficient of $\alpha = 0.2\ dB\ km^{-1}$.

Funding. Tel Aviv University Center for Quantum Science and Technology; Israel Science Foundation (969/22).

Acknowledgments. The authors would like to thank Nadav Arbel for his assistance in constructing the setup. They also thank Aviv Karnieli and Ofir Yesharim for their insightful comments and feedback on the article.

Disclosures. The authors declare no conflict of interest.

Data availability. All data, code, and materials used in the analysis are available upon reasonable request.

Supplemental document. See Supplement 1 for supporting content.

Optics EXPRESS

References

1. W. Gerlach and O. Stern, "Der experimentelle Nachweis der Richtungsquantelung im Magnetfeld," Z Phys. **9**, 349–352 (1922).
2. S. Machluf, Y. Japha, and R. Folman, "Coherent Stern–Gerlach momentum splitting on an atom chip," Nat. Commun. **4**(1), 2424 (2013).
3. M. O. Scully, W. E. Lamb, and A. Barut, "Theory of the Stern-Gerlach apparatus," Found. Phys. **17**(6), 575–583 (1987).
4. S. Nic Chormaic, C. Miniatura, O. Gorceix, *et al.*, "Atomic Stern-Gerlach interferences with time-dependent magnetic fields," Phys. Rev. Lett. **72**(1), 1–4 (1994).
5. B. Viaris de Lesegno, J. C. Karam, M. Boustimi, *et al.*, "Stern Gerlach interferometry with metastable argon atoms: an immaterial mask modulating the profile of a supersonic beam," Eur. Phys. J. D **23**(1), 25–34 (2003).
6. M. Boustimi, V. Bocvarski, B. Viaris de Lesegno, *et al.*, "Atomic interference patterns in the transverse plane," Phys. Rev. A **61**(3), 033602 (2000).
7. Y. Aharonov, D. Z. Albert, and L. Vaidman, "How the result of a measurement of a component of the spin of a spin-1/2 particle can turn out to be 100," Phys. Rev. Lett. **60**(14), 1351–1354 (1988).
8. O. Amit, Y. Margalit, O. Dobkowski, *et al.*, "T3 Stern-Gerlach Matter-Wave Interferometer," Phys. Rev. Lett. **123**(8), 083601 (2019).
9. S. Bose, A. Mazumdar, G. W. Morley, *et al.*, "Spin Entanglement Witness for Quantum Gravity," Phys. Rev. Lett. **119**(24), 240401 (2017).
10. R. J. Cook, "Optical Stern-Gerlach effect," Phys. Rev. A **35**(9), 3844–3848 (1987).
11. C. Hang and G. Huang, "Stern-Gerlach effect of weak-light ultraslow vector solitons," Phys. Rev. A **86**(4), 043809 (2012).
12. Y. Guo, L. Zhou, L. M. Kuang, *et al.*, "Magneto-optical Stern-Gerlach effect in an atomic ensemble," Phys. Rev. A **78**(1), 013833 (2008).
13. Q. Liu, N. Li, and C. Tan, "All-optical logic gate based on manipulation of surface polaritons solitons via external gradient magnetic fields," Phys. Rev. A **101**(2), 023818 (2020).
14. S. Edelstein, R. M. Abraham-Ekeroth, P. A. Serena, *et al.*, "Magneto-optical Stern-Gerlach forces and nonreciprocal torques on small particles," Phys. Rev. Res. **1**(1), 013005 (2019).
15. L. Karpa and M. Weitz, "A Stern–Gerlach experiment for slow light," Nat. Phys. **2**(5), 332–335 (2006).
16. T. Sleator, T. Pfau, V. Balykin, *et al.*, "Experimental demonstration of the optical Stern-Gerlach effect," Phys. Rev. Lett. **68**(13), 1996–1999 (1992).
17. O. Arteaga, E. Garcia-Caurel, and R. Ossikovski, "A Stern-Gerlach experiment with light: separating photons by spin with the method of A. Fresnel," Opt. Express **27**(4), 4758–4768 (2019).
18. N. Kravets, A. Aleksanyan, and E. Brasselet, "Chiral Optical Stern-Gerlach Newtonian Experiment," Phys. Rev. Lett. **122**(2), 024301 (2019).
19. G. Liu, X. Zhang, X. Zhang, *et al.*, "Spin-orbit Rabi oscillations in optically synthesized magnetic fields," Light Sci. Appl. **12**(1), 205 (2023).
20. A. Karnieli and A. Arie, "Frequency domain Stern–Gerlach effect for photonic qubits and qutrits," Optica **5**(10), 1297–1303 (2018).
21. A. Karnieli and A. Arie, "All-Optical Stern-Gerlach Effect," Phys. Rev. Lett. **120**(5), 053901 (2018).
22. O. Yesharim, A. Karnieli, S. Jackel, *et al.*, "Observation of the all-optical Stern–Gerlach effect in nonlinear optics," Nat. Photon. **16**(8), 582–587 (2022).
23. A. Mondal and R. Das, "Experimental evidence of a pump-wavefront-induced Stern–Gerlach-like splitting in optical parametric generators," Opt. Lett. **47**(15), 3668 (2022).
24. H. Suchowski, G. Porat, and A. Arie, "Adiabatic processes in frequency conversion," Laser Photon. Rev. **8**(3), 333–367 (2014).
25. H. Suchowski, D. Oron, A. Arie, *et al.*, "Geometrical representation of sum frequency generation and adiabatic frequency conversion," Phys. Rev. A **78**(6), 063821 (2008).
26. A. Karnieli, S. Tsesses, G. Bartal, *et al.*, "Emulating spin transport with nonlinear optics, from high-order skyrmions to the topological Hall effect," Nat. Commun. **12**(1), 1092 (2021).
27. N. Westerberg, C. Maitland, D. Faccio, *et al.*, "Synthetic magnetism for photon fluids," Phys. Rev. A **94**(2), 023805 (2016).
28. Y. Li, J. Lü, S. Fu, *et al.*, "Geometric representation and the adiabatic geometric phase in four-wave mixing processes," Opt. Express **29**(5), 7288 (2021).
29. X. Ding, D. Heberle, K. Harrington, *et al.*, "Observation of Rapid Adiabatic Passage in Optical Four-Wave Mixing," Phys. Rev. Lett. **124**(15), 153902 (2020).
30. S. Shahnia, B. J. Eggleton, M. J. Collins, *et al.*, "High-efficiency frequency conversion in the single-photon regime," Opt. Lett. **38**(6), 947–949 (2013).
31. S. Clemmen, A. Farsi, S. Ramelow, *et al.*, "Ramsey Interference with Single Photons," Phys. Rev. Lett. **117**(22), 223601 (2016).
32. H. J. McGuinness, M. G. Raymer, C. J. McKinstrie, *et al.*, "Quantum frequency translation of single-photon states in a photonic crystal fiber," Phys. Rev. Lett. **105**(9), 093604 (2010).

Optics EXPRESS

33. A. Karnieli, S. Trajtenberg-Mills, G. Di Domenico, *et al.*, "Experimental observation of the geometric phase in nonlinear frequency conversion," Optica **6**(11), 1401 (2019).
34. A. Karnieli and A. Arie, "Fully controllable adiabatic geometric phase in nonlinear optics," Opt. Express **26**(4), 4920–4932 (2018).
35. E. Bahar, X. Ding, A. Dahan, *et al.*, "Adiabatic four-wave mixing frequency conversion," Opt. Express **26**(20), 25582 (2018).
36. S. Akhmanov, A. Chirkin, K. Drabovich, *et al.*, "Nonstationary nonlinear optical effects and ultrashort light pulse formation," IEEE J. Quantum Electron. **4**(10), 598–605 (1968).
37. W. J. Caputi, "Stretch: A Time-Transformation Technique," IEEE Trans. Aerosp. Electron. Syst. **AES-7**(2), 269–278 (1971).
38. B. H. Kolner and M. Nazarathy, "Temporal imaging with a time lens," Opt. lett. **14**(12), 630–632 (1989).
39. T. Kobayashi, D. Yamazaki, K. Matsuki, *et al.*, "Mach-Zehnder interferometer using frequency-domain beamsplitter," Opt. Express **25**(10), 12052 (2017).
40. P. Imany, O. D. Odele, M. S. Alshaykh, *et al.*, "Frequency-domain Hong–Ou–Mandel interference with linear optics," Opt. Lett. **43**(12), 2760 (2018).
41. T. Kobayashi, R. Ikuta, S. Yasui, *et al.*, "Frequency-domain Hong–Ou–Mandel interference," Nat. Photon. **10**(7), 441–444 (2016).
42. C. Joshi, A. Farsi, A. Dutt, *et al.*, "Frequency-domain quantum interference with correlated photons from an integrated microresonator," Phys. Rev. Lett. **124**(14), 143601 (2020).
43. M. G. Raymer, S. J. van Enk, C. J. McKinstrie, *et al.*, "Interference of two photons of different color," Opt. Commun. **283**(5), 747–752 (2010).
44. M. Kues, C. Reimer, P. Roztocki, *et al.*, "On-chip generation of high-dimensional entangled quantum states and their coherent control," Nature **546**(7660), 622–626 (2017).
45. M. Kues, C. Reimer, J. M. Lukens, *et al.*, "Quantum optical microcombs," Nat. Photon. **13**(3), 170–179 (2019).
46. R. W. Boyd, *Nonlinear Optics* (Academic Press, 2008).
47. G. P. Agrawal, *Nonlinear Fiber Optics* (Academic Press, 2012).
48. F. Casas, A. Murua, and M. Nadinic, "Efficient computation of the Zassenhaus formula. Comput," Phys. Commun. **183**(11), 2386–2391 (2012).
49. T. Okoshi, K. Kikuchi, and A. Nakayama, "Novel method for high resolution measurement of laser output spectrum," Electron. Lett. **16**(16), 630–631 (1980).
50. Y. H. Li, S. L. Li, and X. L. Hu, "Free-Space and Fiber-Integrated Measurement-Device-Independent Quantum Key Distribution under High Background Noise," Phys. Rev. Lett. **131**(10), 100802 (2023).
51. D. J. Shepherd, "On the role of Hadamard Gates in quantum circuits," Quantum Inf Process **5**(3), 161–177 (2006).
52. H. H. Lu, J. M. Lukens, N. A. Peters, *et al.*, "Electro-optic frequency beam splitters and tritters for high-fidelity photonic quantum information processing," Phys. Rev. Lett. **120**(3), 030502 (2018).
53. R. A. Fisher and W. K. Bischel, "Numerical studies of the interplay between self-phase modulation and dispersion for intense plane-wave laser pulses," J. Appl. Phys. **46**(11), 4921–4934 (1975).
54. R. A. Fisher and W. K. Bischel, "The role of linear dispersion in plane-wave self-phase modulation," Appl. Phys. Lett. **23**(12), 661–663 (1973).